Diode laser lidar wind velocity sensor using a liquid-crystal retarder for non-mechanical beam-steering

Rodrigo, Peter John; Iversen, Theis Faber Quist; Hu, Qi; Pedersen, Christian

Published in:
Optics Express

Link to article, DOI:
10.1364/OE.22.026674

Publication date:
2014

Document Version
Publisher's PDF, also known as Version of record

Diode laser lidar wind velocity sensor using a liquid-crystal retarder for non-mechanical beam-steering

Peter John Rodrigo,[1,*] Theis F. Q. Iversen,[2] Qi Hu,[1] and Christian Pedersen[1]

[1]*DTU Fotonik, Department of Photonics Engineering, Technical University of Denmark, 4000 Roskilde, Denmark*
[2]*Windar Photonics A/S, Helgeshøj Alle 16-18, 2630 Taastrup, Denmark*
[*]*pejr@fotonik.dtu.dk*

Abstract: We extend the functionality of a low-cost CW diode laser coherent lidar from radial wind speed (scalar) sensing to wind velocity (vector) measurements. Both speed and horizontal direction of the wind at ~80 m remote distance are derived from two successive radial speed estimates by alternately steering the lidar probe beam in two different lines-of-sight (LOS) with a 60° angular separation. Dual-LOS beam-steering is implemented optically with no moving parts by means of a controllable liquid-crystal retarder (LCR). The LCR switches the polarization between two orthogonal linear states of the lidar beam so it either transmits through or reflects off a polarization splitter. The room-temperature switching time between the two LOS is measured to be in the order of 100 μs in one switch direction but 16 ms in the opposite transition. Radial wind speed measurement (at 33 Hz rate) while the lidar beam is repeatedly steered from one LOS to the other every half a second is experimentally demonstrated – resulting in 1 Hz rate estimates of wind velocity magnitude and direction at better than 0.1 m/s and 1° resolution, respectively.

OCIS codes: (010.3640) Lidar; (140.5960) Semiconductor lasers; (230.3720) Liquid-crystal devices.

References and links

1. R. S. Hansen and C. Pedersen, "All semiconductor laser Doppler anemometer at 1.55 μm," Opt. Express **16**(22), 18288–18295 (2008).
2. P. J. Rodrigo and C. Pedersen, "Doppler wind lidar using a MOPA semiconductor laser at stable single-frequency operation," in *Technical Digest. 19th International Congress on Photonics in Europe, CLEO/Europe-EQEC* (2009).
3. P. J. Rodrigo and C. Pedersen, "Field performance of an all-semiconductor laser coherent Doppler lidar," Opt. Lett. **37**(12), 2277–2279 (2012).
4. P. J. M. Clive, "Lidar and resource assessment for wind power applications: the state of the art," Proc. SPIE **7111**, 711107 (2008).
5. M. Harris, M. Hand, and A. Wright, "Lidar for turbine control," Technical Report NREL/TP-500–39154, NREL, January 2006.
6. E. Simley, L. Y. Pao, P. Gebraad, and M. Churchfield, "Investigation of the impact of the upstream induction zone on LIDAR measurement accuracy for wind turbine control applications using large-eddy simulation," J. Phys. Conf. Ser. **524**, 012003 (2014).
7. M. Harris, G. N. Pearson, J. M. Vaughan, D. Letalick, and C. J. Karlsson, "The role of laser coherence length in continuous-wave coherent laser radar," J. Mod. Opt. **45**(8), 1567–1581 (1998).
8. Q. Hu, P. J. Rodrigo, and C. Pedersen, "Remote wind sensing with a CW diode laser lidar beyond the coherence regime," Opt. Lett. **39**(16), 4875–4878 (2014).

1. Introduction

As light sources of coherent lidar systems for wind sensing, narrow-linewidth semiconductor (diode) lasers operating in the eye-safe telecom wavelength regime (λ ~1.55 μm) have been proven as compact and cheaper alternative to fiber lasers [1–3]. These attractive features can

#213496 - $15.00 USD Received 8 Aug 2014; revised 13 Oct 2014; accepted 14 Oct 2014; published 21 Oct 2014

potentially be used as leverage for developing cost-efficient lidar sensors for the wind energy industry, which is becoming more and more interested in laser Doppler anemometry applications from wind resource assessment (both in development and operational sites) [4] to wind turbine control [5, 6]. The advantages are derived from the fact that diode lasers are readily mass-producible through the well-established microelectronics fabrication technology. Furthermore, a fiber laser customarily needs to work in tandem with an additional optical amplifier (e.g. erbium-doped fiber amplifier) to achieve the required average CW output power in wind lidars – typically ~1 W. This power level is now achievable with a single chip-integrated master-oscillator (tapered) power-amplifier semiconductor laser (MOPA-SL) [2].

The linewidth of diode laser is typically broader than that of fiber lasers. Nonetheless, previous laboratory investigations into diode laser linewidth requirements in CW coherent lidar have found that measurement at distances beyond the coherence region is still feasible if the laser phase fluctuations are overwhelmed by target speckle fluctuations [7]. This means that modest laser linewidth comparable to the target speckle bandwidth can be used even at probing distances outside the traditional coherence region. We have recently verified this for aerosol target (characterized by 1 - 2 MHz speckle bandwidth) by experimentally comparing the performance of two CW coherent MOPA-SL lidars with both systems measuring the radial wind speed at ~85 m distance. One lidar has a laser linewidth comparable to the target speckle bandwidth and the other lidar has an order of magnitude narrower linewidth [8].

All previous demonstrations of our MOPA-SL based CW coherent lidar have been limited to single line-of-sight (LOS) measurements [1–3, 8]. Hence, only the scalar radial wind speed component can be measured by the lidar. In this work, we design and implement an improved wind sensor that extends the functionality of our MOPA-SL wind lidar to measurements of both magnitude and direction of the wind velocity (vector). The vector measurement principle as well as the design, implementation, and experimental characterization of the enhanced lidar are discussed in the following sections.

2. Operational principle of the dual-LOS wind lidar

To extend the lidar functionality to measure both wind speed and azimuthal direction, a two-LOS laser wind sensor (which we named “WindEye”) is proposed as shown in Fig. 1. It is an improved version of the single-LOS diode laser lidar and is subdivided into two modules: an optical transceiver head and a control unit. Like its predecessor (e.g. setup in our previous work [3]), the WindEye’s optical transceiver incorporates an optical circulator to: (1) transmit

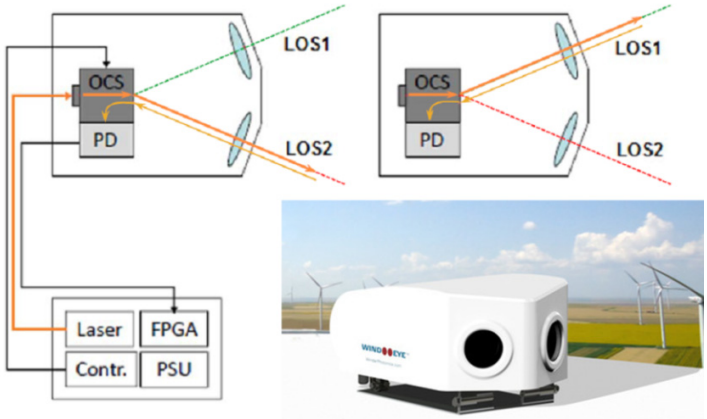

Fig. 1. The WindEye – a dual-LOS wind lidar. It makes use of an optical circulator/switch (OCS) to non-mechanically steer the transmitted laser beam to either LOS1 or LOS2 and to direct the received backscatter to the photodetector (PD). A field-programmable gate array (FPGA) unit calculates the lidar signal power spectra. The laser, controllers, power supply unit (PSU) and FPGA-based data processor are linked to the two-eyed optical transceiver by 10 m long fiber and electrical cables. The inset shows a sketch of the WindEye mounted on a turbine.

#213496 - $15.00 USD Received 8 Aug 2014; revised 13 Oct 2014; accepted 14 Oct 2014; published 21 Oct 2014

a large fraction of the laser power (~500 mW) to the target, (2) tap a tiny fraction (~0.1%) of the laser power to form a local oscillator, and (3) direct the local oscillator and the Doppler shifted target-backscatter radiation to a photodetector. Power spectral density (PSD) plots from 512-point time series (75 MHz sampling) of the photodetector output signal (i.e. beat signal oscillating at mean Doppler shift frequency f_D) are averaged to estimate the radial speed v_{LOS} at 33 Hz rate using:

$$v_{LOS} = \frac{\lambda}{2} f_D. \quad (1)$$

To maintain our lidar's advantages (i.e. low cost and simplicity), we have come up with an optical design that circumvents the duplication of key lidar subcomponents except for the telescope. The WindEye employs two fixed-focus telescopes (each focus at ~85 m distance with a probe length of ~25 m) for launching laser beams interchangeably in two horizontal lines-of-sight (LOS1 and LOS2) with 60° separation angle. A pair of successive measurements of v_{LOS1} and v_{LOS2} consequently allows for estimation of both magnitude and direction of the wind vector using simple trigonometry. This method increases in accuracy if the wind flow is more laminar – such as those typically found at hub height in flat terrain and offshore wind farms. We envision the use of a WindEye mounted on the turbine's nacelle to preview the changes in the average direction of the incoming wind for improved yaw control. Other commercially available wind lidar systems incorporate the speed-and-direction functionality into their products (e.g. ZephIR of Natural Power and Galion of SgurrEnergy) by means of mechanical beam-scanners [5]. ZephIR is based on rotating (Risley) prisms while Galion relies on a pair of mirrors independently turned around two orthogonal axes. Both motorized beam-scanners are however expensive, bulky and prone to wear and tear. Our approach makes use of a low-cost non-mechanical beam-steering system based on a few off-the-shelf optical components as illustrated in Fig. 2. Using a controllable liquid-crystal retarder (LCR), a polarization beam splitter and a pair of stationary mirrors, a beam-steering function is integrated with the optical circulator – creating an optical circulator/switch.

The LCR acts as a half-wave plate when a 2 kHz square wave drive voltage, ~1.5 V (rms), is applied – changing the incident linear p-polarized beam to an s-polarized beam that is reflected off the beam splitter. The input p-polarized beam is unchanged by the LCR and

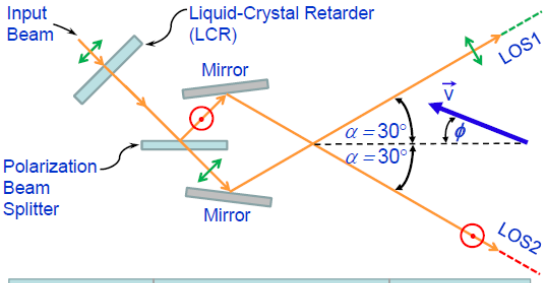

LCR Voltage	LCR Output Polarization	Active Beam
~1.5 V (rms)	⊙ s-polarized	LOS2
25 V (rms)	↕ p-polarized	LOS1

Fig. 2. Non-mechanical beam-steering system with a liquid-crystal retarder (LCR). The LCR with a 10 mm clear aperture is electronically addressed to either preserve the input beam polarization state (p-polarized for high LCR drive voltage) or change it to its orthogonal counterpart (s-polarized for low drive voltage). p-polarized (/s-polarized) beam is transmitted through (/reflected off) the polarization beam splitter and deflected by a mirror to send the beam along LOS1 (/LOS2). Both LOS1 (green dashed line) and LOS2 (red dashed line) make an angle $\alpha = 30°$ with the lidar axis (black dashed line). A blue arrow illustrates a possible orientation of the wind velocity vector $\vec{v}$ with an azimuthal direction ϕ relative to the lidar axis (ϕ is positive for this particular example).

#213496 - $15.00 USD Received 8 Aug 2014; revised 13 Oct 2014; accepted 14 Oct 2014; published 21 Oct 2014

transmitted through the beam splitter if the drive voltage is 25 V (rms). Thus, measurement of v_{LOS2} is activated by the low LCR voltage while measurement of v_{LOS1} gets triggered by the high LCR voltage. According to its specification, the LCR has a wavefront distortion of $\leq \lambda/10$ and an insertion loss of 0.2 dB (single pass). Both are sufficiently low and allow us to maintain good heterodyne efficiency as exemplified by the results below. The 0.5 W incident beam onto the LCR is collimated to a $1/e^2$ diameter of 2 mm resulting in a power density well below the LCR damage threshold of 500 W/cm^2 specified by the manufacturer.

For every pair of (positive-valued) v_{LOS1} and v_{LOS2} estimates, the magnitude $|\vec{v}|$ and direction ϕ of the wind velocity vector shown in Fig. 2 can be derived by solving a system of two equations (to avoid ambiguity, we assume $\alpha - \pi/2 < \phi < \pi/2 - \alpha$ where α shown in Fig. 2 is always positive). The first equation gives the projection of vector $\vec{v}$ onto the lidar axis:

$$|\vec{v}|\cos\phi = \frac{(v_{LOS1} + v_{LOS2})}{2\cos\alpha}, \tag{2}$$

and the other supplies the component along the orthogonal direction:

$$|\vec{v}|\sin\phi = \frac{(v_{LOS2} - v_{LOS1})}{2\sin\alpha}. \tag{3}$$

For $\alpha = 30°$, $|\vec{v}|\cos\phi = \sqrt{3}(v_{LOS1} + v_{LOS2})/3$ and $|\vec{v}|\sin\phi = v_{LOS2} - v_{LOS1}$.

3. Characterization of the LCR based beam-steering system

To evaluate the switching characteristics of the new dual-LOS lidar, we measured the optical power of the beam transmitted out of the two telescope exit apertures (Fig. 1) as the LCR is repeatedly switched between the two LOS every half a second. The alternating modulation of the beam power for LOS1 and LOS2 is shown in Fig. 3 with the corresponding LCR drive voltage. These results show that the switching time constants to reroute the transmitted beam from LOS1 to LOS2 is longer (τ_{12} = 16 ms) than for the opposite direction (τ_{21} = 100 µs). It is worth to note that next-generation LCRs with stabilizing polymer materials are already commercially available and can provide switching speeds in the order of 100 µs in both directions. Nonetheless, the present asymmetry in the switching time constants is not critical in our current system, since the target update rate is in the order of 1 Hz for wind field magnitude and direction measurement.

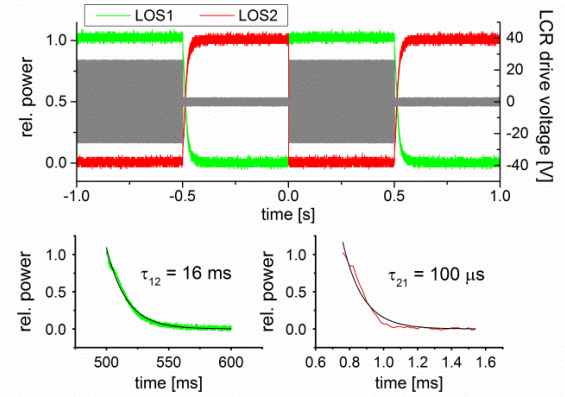

Fig. 3. (Top) Measured relative power of the laser beam versus time, alternately transmitted along LOS1 (green) and LOS2 (red), along with the corresponding LCR drive voltage (gray) that enables this non-mechanical lidar beam-steering mechanism. (Bottom) Time constants for switching the beam from LOS1 to LOS2 and vice versa (i.e. τ_{12} and τ_{21}) are estimated by fitting exponential decay curves to the relative beam power transitions at 0.5 s and 0.0 s, respectively. The measurements were performed at an ambient temperature of 25 °C.

#213496 - $15.00 USD Received 8 Aug 2014; revised 13 Oct 2014; accepted 14 Oct 2014; published 21 Oct 2014

As shown in Fig. 1, a field-programmable gate array (FPGA) unit is used to perform real-time lidar spectral analysis. The FPGA continuously calculates the PSD of the photodetector signal every 6.83 μs (a sampling rate of 75 MHz consisting 512 sample points) and averages a few thousands of these spectra to produce 33 Hz PSD plots regardless of the LCR's state. Two examples of the 33 Hz PSD plots are illustrated in Fig. 4. The first plot is for the case when the LCR drive voltage is high (i.e. LOS1 is active) and the second is when the LCR drive voltage is low (LOS2 is active). The former gives a mean f_D = 5 MHz while the latter clearly has a lower f_D = 3 MHz which is indicative that the wind velocity vector is more closely aligned along LOS1 than along LOS2. As can be predicted from Fig. 3, it is observed that some 33 Hz PSD plots generated at times very close to the switch transitions contain two Doppler peaks that actually mixed the individual peaks from the LOS1 and the LOS2 measurements. This ambiguous situation (or crosstalk) occurs often for the slow transition (LOS1 to LOS2) but is also observed in the opposite switch direction. To mitigate this issue, a filtering algorithm is introduced which simply drops two 33 Hz PSD plots for every switching event – one before and one after a transition. A 10 s video clip of the 33 Hz PSD plots while the LCR is alternately switched is linked to Fig. 4 and shows the result after applying the filtering algorithm.

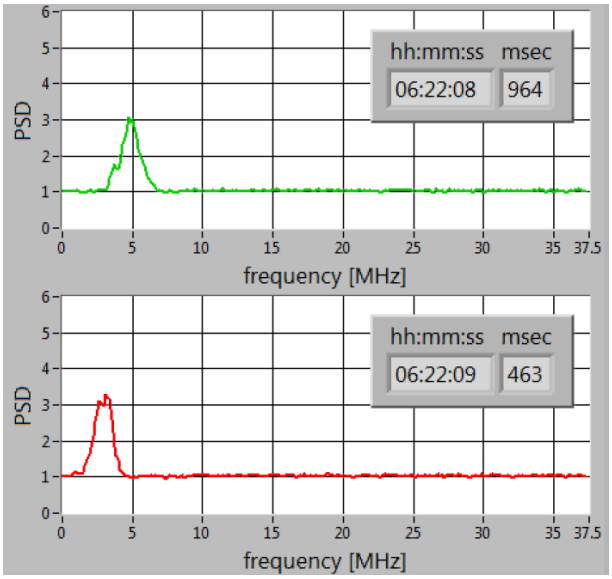

Fig. 4. Power spectral density (PSD) of the lidar photodetector output signal when LOS1 is active (top) and when the lidar switches to LOS2 (bottom). PSD plots are given in units of the shot noise background. For each LOS, the radial wind speed is directly proportional to the estimated center frequency of the Doppler peak (e.g. 5 MHz for LOS1 and 3 MHz for LOS2 for the above plots). The time stamp of each plot is shown on their upper right corner. An accompanying video clip (Media 1) is included to show the 33 Hz lidar spectra for a period of 10 s while the beam switches from one LOS to another every half a second. Assuming laminar flow, equal radial wind speeds are obtained when the wind vector is parallel to the lidar axis (or symmetry axis between LOS1 and LOS2).

4. Determining the wind velocity vector (magnitude and direction)

An outdoor experiment is performed during which the wind direction is mostly within the 60° sector defined by LOS1 and LOS2 of the WindEye lidar system. After applying the abovementioned filtering algorithm to the 33 Hz PSD plots gathered during the experiment, a large fraction of the total lidar data remains and is used to generate 1 Hz averages of v_{LOS1} and v_{LOS2} using Eq. (1). The temporal variations of v_{LOS1} and v_{LOS2} over a 50 minute period are shown in Fig. 5 (top). Using Eq. (2) and Eq. (3), the corresponding magnitude $|\vec{v}|$ and

#213496 - $15.00 USD Received 8 Aug 2014; revised 13 Oct 2014; accepted 14 Oct 2014; published 21 Oct 2014

direction ϕ of the wind velocity vector are also plotted in Fig. 5 (bottom). The data shows that for the first half hour, v_{LOS1} is mostly greater than v_{LOS2} (resulting in $\phi < 0$) until around 06:38 when the two plots cross over (corresponding to $\phi = 0$). For the remainder, the situation is reversed (i.e. $\phi > 0$). Astute readers can further note two outlying data points for the relative wind direction (+ 60° at around 06:18 and –60° at 06:40). These outliers can be ignored since they correspond to instances when zero values are assigned by default to v_{LOS1} and/or v_{LOS2} when the lidar spectra have poor signal-to-noise ratio, which makes radial speed estimates unreliable. For yaw control applications, the objective is to minimize $|\phi|$ assuming that the lidar axis is well aligned with the rotor axis of the turbine. A further examination of the 1 Hz data also shows that the achieved resolution is less than 0.1 m/s for the velocity magnitude and better than 1° for the wind direction.

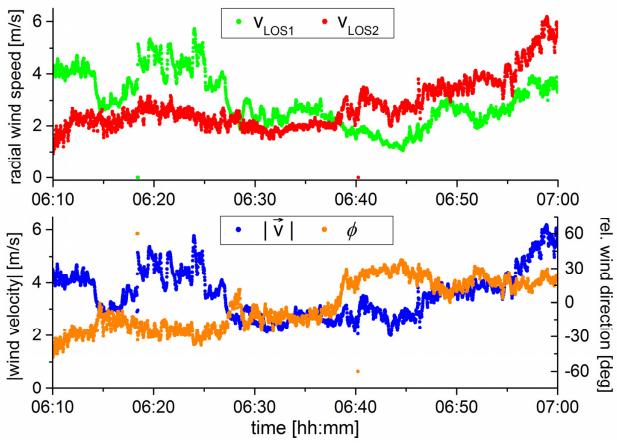

Fig. 5. Plots of the 1 Hz radial wind speed data for LOS1 and LOS2 (top) and the corresponding estimates for the magnitude and direction (measured relative the lidar axis) of the wind velocity vector. Time axis is in units of hours:minutes.

5. Conclusion and outlook

We have demonstrated a novel diode laser wind lidar with a dual line-of-sight beam-steering capability without moving parts. Non-mechanical steering of the beam is accomplished by a liquid-crystal polarization switch working in conjunction with a polarization beam splitter. This work demonstrates that successive pairs of spatially resolved radial speed measurements along two horizontal lines-of-sight at –30° and + 30° of the lidar symmetry axis can be used to determine the magnitude and direction of the wind velocity vector at a remote distance (nearly 100 m away from the instrument), assuming a relatively laminar flow. As a further extension of this work, we are in the process of validating the performance of the low-cost diode laser wind *velocity* lidar over extended periods (i.e. months) and under various meteorological conditions by conducting side-by-side comparison with state-of-the-art sonic anemometers as reference in situ wind sensors. The non-mechanical beam-steering scheme demonstrated here for a CW lidar can also be applied to a pulsed lidar as long as the energy density of the beam incident on the liquid-crystal retarder is less than the damage threshold of the device. Lastly, the dual-LOS lidar may also be used to measure light depolarization by atmospheric particles.

Acknowledgment

The authors would like to acknowledge the financial support from the Energiteknologisk Udviklings- og Demonstrations Program (EUDP) J.nr. 641012-0003.